Stomatal control of leaf fluxes of carbonyl sulfide and CO_2 in a *Typha* freshwater marsh

Wu Sun[1], Kadmiel Maseyk[2,a], Céline Lett[3,a], and Ulli Seibt[1,a]

[1]Department of Atmospheric and Oceanic Sciences, University of California, Los Angeles, CA 90095-1565, USA
[2]School of Environment, Earth and Ecosystem Sciences, The Open University, Milton Keynes MK7 6AA, United Kingdom
[3]Laboratoire des Sciences du Climat et de l'Environnement, Université Paris Saclay, 91191 Gif-sur-Yvette, France
[a]formerly at Institute of Ecology and Environmental Sciences, Université Pierre et Marie Curie Paris 6, France

Correspondence: Wu Sun (wu.sun@ucla.edu) and Ulli Seibt (useibt@ucla.edu)

Abstract. Carbonyl sulfide (COS) is an emerging tracer to constrain land photosynthesis at canopy to global scales, because leaf COS and CO_2 uptake processes are linked through stomatal diffusion. The COS tracer approach requires knowledge of the concentration normalized ratio of COS uptake to photosynthesis, commonly known as the leaf relative uptake (LRU). LRU is known to increase under low light, but the environmental controls over LRU variability in the field are poorly understood due to scant leaf scale observations.

Here we present the first direct observations of LRU responses to environmental variables in the field. We measured leaf COS and CO_2 fluxes at a freshwater marsh in summer 2013. Daytime leaf COS and CO_2 uptake showed similar peaks in the mid-morning and late afternoon separated by a prolonged midday depression, highlighting the common stomatal control on diffusion. At night, in contrast to CO_2, COS uptake continued, indicating partially open stomata. LRU ratios showed a clear relationship with photosynthetically active radiation (PAR), converging to 1.0 at high PAR, while increasing sharply at low PAR. Daytime integrated LRU (calculated from daytime mean COS and CO_2 uptake) ranged from 1 to 1.5, with a mean of 1.2 across the campaign, significantly lower than previously reported laboratory mean value (~1.6). Our results indicate two major determinants of LRU—light and vapor deficit. Light is the primary driver of LRU because CO_2 assimilation capacity increases with light, while COS consumption capacity does not. Superimposed upon the light response is a secondary effect that high vapor deficit further reduces LRU, causing LRU minima to occur in the afternoon, not at noon. The partial stomatal closure induced by high vapor deficit suppresses COS uptake more strongly than CO_2 uptake because stomatal resistance is a more dominant component in the total resistance of COS. Using stomatal conductance estimates, we show that LRU variability can be explained in terms of different patterns of stomatal vs. internal limitations on COS and CO_2 uptake. Our findings illustrate the stomata-driven coupling of COS and CO_2 uptake during the most photosynthetically active period in the field and provide an in-situ characterization of LRU—a key parameter required for the use of COS as a photosynthetic tracer.

1 Introduction

Carbonyl sulfide (COS) is a unique tracer for land photosynthesis (i.e., gross primary productivity, GPP) at regional to global scales (e.g., Montzka et al., 2007; Campbell et al., 2008; Berry et al., 2013; Campbell et al., 2017). Globally, COS is mainly emitted from the ocean and anthropogenic activities and consumed by leaves and soils (Berry et al., 2013; Launois et al., 2015; Campbell et al., 2015; Whelan et al., 2017). Since ecosystem COS exchange is dominated by plant uptake (Berry et al., 2013), concurrent measurements of COS and CO_2 fluxes can be used to separate photosynthesis and respiration from the net carbon flux (e.g., Asaf et al., 2013; Billesbach et al., 2014). Understanding the quantitative relationship between leaf COS and CO_2 fluxes is therefore critical to estimating canopy and regional photosynthesis from COS measurements.

In leaves, COS and CO_2 follow the same stomatal diffusional pathway and similar hydrolytic reactions catalyzed by carbonic anhydrase (CA), with the main difference being that the hydrolysis goes reversibly for CO_2 but one-way for COS (Protoschill-Krebs et al., 1996; Notni et al., 2007). The reaction of COS with CA yields H_2S and CO_2 (Schenk et al., 2004; Notni et al., 2007), without any observed COS (re)-emission from leaves (Stimler et al., 2010). In contrast, CO_2 hydration is subject to chemical equilibrium that depends on its diffusional supply versus its demand from fixation, leading to retrodiffusion to the atmosphere. CA-mediated hydrolysis therefore serves as the sink reaction of COS in leaves, but not of CO_2.

The COS hydrolysis via CA is light independent (Goldan et al., 1988; Protoschill-Krebs et al., 1996). Since this reaction is also highly efficient (Ogawa et al., 2013), COS uptake rate should be mostly controlled by the sequence of conductances along the diffusional pathway into leaves, i.e., substrate limited rather than enzyme limited (Goldan et al., 1988; Sandoval-Soto et al., 2005; Seibt et al., 2010; Stimler et al., 2010). Leaf COS uptake should therefore respond to environmental variables that regulate diffusion—mainly stomatal diffusion—including photosynthetically active radiation (PAR), because of the feedback from photosynthesis to stomatal conductance (Ball, 1988; Collatz et al., 1991), and vapor deficit (Leuning, 1995). Thus, light regulates leaf COS uptake even though COS hydrolysis itself does not depend on light.

At night, in contrast to the CO_2 emission, COS uptake may continue if stomata are not fully closed (Stimler et al., 2010). To understand the relationship between daily integrated COS and CO_2 fluxes for regional flux inversion (e.g., Hilton et al., 2015), nighttime COS uptake needs to be constrained (Maseyk et al., 2014). Nighttime COS uptake has been observed in a wheat field (Maseyk et al., 2014), a boreal pine forest (Kooijmans et al., 2017), and temperate forests (Berkelhammer et al., 2014; Commane et al., 2015; Wehr et al., 2017). Most field studies base their findings of nighttime COS uptake upon ecosystem scale observations, with only one study reporting nighttime COS uptake at the leaf scale (Berkelhammer et al., 2014).

The quantitative relationship between leaf COS uptake and photosynthesis required for COS-based photosynthesis estimates—from canopy to regional scales (e.g., Asaf et al., 2013; Hilton et al., 2017)—is commonly expressed in one parameter: leaf relative uptake (LRU). LRU is the ratio of leaf COS : CO_2 fluxes normalized by their respective ambient concentrations (Sandoval-Soto et al., 2005; Campbell et al., 2008). A mean LRU value of 1.6 has been reported for a wide range of species from leaf scale measurements in the laboratory (Stimler et al., 2010, 2011, 2012) and the field (Berkelhammer et al., 2014). But in the field, lower LRU values have also been observed, e.g., 1.3 in a wheat field (Maseyk et al., 2014) and 1.2 in a temperate forest (Commane et al., 2015), both estimated from ecosystem scale measurements.

For ecosystem scale applications, a constant LRU of 1.6 has been assumed (e.g., Asaf et al., 2013) despite the known dependence of LRU on PAR. LRU is found to decrease with light in both laboratory and field observations (Stimler et al., 2010, 2011; Maseyk et al., 2014; Commane et al., 2015). Leaf level measurements in the laboratory show that LRU is stable at PAR above ca. 500 μmol m^{-2} s^{-1}, but increases sharply with decreasing PAR (Stimler et al., 2010, 2011). The stable LRU region is consistent with that of light-saturated photosynthesis and maximal stomatal conductance, and therefore low variations in COS and CO_2 fluxes (Stimler et al., 2011). At low light, the extent to which LRU increases differs among species, with some showing a sharp increase to LRU values of ca. 9, while others show a more gradual or only slight increase. This LRU behavior results from the diverging responses of COS and CO_2 uptake in low light: CO_2 assimilation that is also controlled by light decreases more rapidly than COS uptake that is only controlled by stomatal conductance. Using a light dependent LRU instead of a constant value is therefore necessary for COS-based photosynthesis estimates. But in the field, the LRU–PAR relationship has only been approximated with ecosystem fluxes (Maseyk et al., 2014; Commane et al., 2015), not directly determined from leaf fluxes. For COS-based canopy photosynthesis estimates, we need direct measurements of how LRU responds to PAR and other possible drivers in the field. Applications at longer timescales would further need daily integrated LRU values.

This study aims to characterize how light and vapor deficit drive variabilities in leaf COS uptake and LRU and to probe the stomatal mechanism that underlies LRU responses to these drivers. Here, we hypothesize that (i) light dependence of instantaneous LRU is analogous to that reported in laboratory conditions, and this relationship is also preserved in daily integrated LRU; and (ii) strong diurnal variation of vapor deficit will have observable effects on COS uptake and LRU, due to stomatal response to vapor deficit. We report leaf COS and CO_2 fluxes measured in a *Typha latifolia* freshwater marsh during the peak growing season of June and July 2013. We then examine how environmental variables control fluxes and LRU through stomatal mechanisms, and discuss the implications for COS-based photosynthesis estimates.

2 Methods

2.1 Site description

We measured leaf fluxes of COS, CO_2, and water from 31 May to 6 July 2013 (day of year 151–187) at the San Joaquin Freshwater Marsh (SJFM, 33°39′44.4″ N, 117°51′6.1″ W). The SJFM is located near the campus of the University of California, Irvine, at 3 m above sea level and 8 km northeast of the Pacific Ocean (Goulden et al., 2007). The SJFM is part of the University of California's Natural Reserve System. The site history and management have been described in Goulden et al. (2007). Briefly, the SJFM is a mature freshwater marsh, the remnant of once a 2100 ha wetland along the San Diego Creek. Since the 1960s, the SJFM has been managed by flooding the area annually to a depth of approximately 1 m from December/January to March. The standing water recedes by evapotranspiration and subsurface drainage and eventually disappears by midsummer (Goulden et al., 2007). A flux tower (5 m tall) is located on a floating wooden platform near the northeastern edge of the SJFM. The platform is surrounded by dense vegetation dominated by *Typha latifolia* (broadleaf cattail). In contrast to most species in a mediterranean climate that grow in the rainy winter or early spring, the growing season of the marsh plants is summer due to the standing water.

2.2 Experimental setup

Leaf fluxes of COS, CO_2, and H_2O were measured with a flow-through (dynamic) chamber (Fig. 1a). The cylindrical chamber (18 cm diameter, 38 cm height, 10.3 L volume) consisted of PFA Teflon film stretched between two aluminum rings connected by rods. The PFA film was laid inside the structure such that only the film was in contact with the sampled air. The chamber enclosed the upper sections of six tall *T. latifolia* leaves with an average width of 1.5 cm. The leaves extended above and below the chamber. The total leaf area in the chamber was estimated as 409.5 cm^2. Skirts of Teflon film were wrapped around the leaves to provide a seal at both ends of the chamber.

Two fans were installed in the chamber for ventilation and mixing, respectively. On the inlet end, a high-speed axial fan (D344T, Micronel; 40×40 mm) provided ventilation to keep the chamber at ambient conditions (i.e., within 1 ppmv of ambient CO_2, tested at the start of the campaign). A second, smaller flat fan (F62, Micronel; 16 × 16 mm), attached to a stainless steel rod, was placed near the center of the chamber for air mixing. During the measurement period, the ventilation fan was turned off and its opening served as the inlet to allow airflow through the chamber. The mixing fan, in contrast, was kept running at all times.

The chamber was connected via a 0.25-inch PFA Teflon tubing to a Quantum Cascade Laser (QCL) analyzer (CW-QC-TILDAS, Aerodyne Research Inc., Billerica, MA, USA), with a 1 µm Teflon filter attached at the inlet of the analyzer. The analyzer was placed in an instrument enclosure on the platform. Flow through the analyzer was provided by a Varian TriScroll 600 pump (Agilent Technologies Inc., Santa Clara, CA, USA). Flow rate in the sampling tube was 6.4 standard liter per minute (slm), which corresponded to a chamber air turnover time of around 1.5 minutes. The pump was placed next to the nearest main power line near the entrance to the marsh site, and connected to the analyzer by a 150 m long 2-inch vacuum line. A solenoid valve at the inlet to the QCL was used to switch from the sampling line to a stream of dry N_2 (ultrahigh purity) for a one-minute background correction every hour. Data from the QCL analyzer were recorded at 10 Hz and stored on the QCL hard drive. The root-mean-square deviation of COS measurements at 10 Hz was 11–18 parts per trillion in volume (pptv).

Correction for water vapor effects on the dry mixing ratios of COS and CO_2 was done in the TDLWintel data acquisition software on the analyzer (Nelson, 2012). We did not use the same correction factors reported in Kooijmans et al. (2016) for the same make of QCL analyzer; however, a mock run of data processing with CO_2 concentration recalculated using their correction factor value resulted in a potential bias of only 0.12% (r^2 = 0.999). Thus, the flux uncertainty associated with the correction factor of water vapor effects was negligible (see the Supplement for details).

The leaf chamber was measured once per hour. Chamber operations were programmed on a CR1000 datalogger (Campbell Scientific, Inc., Logan, UT, USA). We monitored chamber air concentrations for a five-minute measurement period (i.e., while the ventilation fan was off), as well as the ambient air for one minute before and after measurement periods (i.e., while the ventilation fan was running). Leaf fluxes were calculated from the transient changes with respect to the interpolated inlet (ambient) concentrations (Fig. 1b). The apparent fluxes from the chamber material (PFA), characterized post hoc, were negligible—the blank effects translated to apparent fluxes of 0.05 ± 0.29 pmol m^{-2} s^{-1} for COS and 0.02 ± 0.15 µmol m^{-2} s^{-1} for CO_2 when normalized against the leaf area (see the Supplement).

Various sensors were installed to record environmental data, including photosynthetically active radiation (PAR) (SQ-215, Apogee Instruments), ambient air temperature and humidity (HMP45AC, Vaisala), and chamber air and leaf temperature (type T thermocouples, PFA coated). These data were recorded at 10 s intervals on the CR1000 datalogger. The PAR sensor was placed near the chamber to measure the light microenvironment of the chamber. All sensor data are released alongside the flux data (see Data Availability).

2.3 Calculation of leaf fluxes

A mass balance equation is formulated for the gas species being measured (COS, CO_2, or H_2O),

$$V\frac{\mathrm{d}C}{\mathrm{d}t} = q\,(C_\mathrm{a} - C) + FA \tag{1}$$

where C (mol m^{-3}) is the chamber headspace concentration of the gas, C_a (mol m^{-3}) is the inlet (ambient) concentration, q ($\mathrm{m}^3\ \mathrm{s}^{-1}$) is the inlet flow rate, V (m^3) and A (m^2) are the chamber volume and leaf area, respectively, and F (mol $\mathrm{m}^{-2}\ \mathrm{s}^{-1}$) is the flux rate to be calculated. Solving the mass balance equation with the initial condition $C(t = 0) = C_\mathrm{a}$, we obtain

$$C\,(t) = -\frac{FA}{q}\exp(-qt/V) + C_\mathrm{a} + \frac{FA}{q} \tag{2}$$

The flux rate F is

$$F = \frac{q}{A}\cdot\frac{C - C_\mathrm{a}}{1 - \exp(-qt/V)} \tag{3}$$

Let $\hat{y} = C - C_\mathrm{a}$ and $\hat{x} = \exp(-qt/V)$ be the variables for the regression, hence,

$$\hat{y} = \frac{FA}{q}\,(1 - \hat{x}) \tag{4}$$

The flux rate F is then solved from the slope of the regression $\hat{y} \sim (1 - \hat{x})$. The standard error of the estimated F is also obtained from the regression. The flux calculation method described above does not require a steady state to be reached in the chamber. A typical example of the chamber measurement period with the fitted curve of COS concentration changes is shown in Fig. 1b.

2.4 Data quality control

All leaf flux and meteorological data have been quality checked and filtered. Conspicuously unrealistic data points in the meteorological data were removed. For the flux data, we used several independent criteria to filter measurements. First, measurement periods with serious misfit of the shape of concentration changes during chamber closure or with strong drift in the ambient concentrations were discarded. Second, flux estimates associated with large root-mean-square errors between fitted and observed concentrations were also discarded. Then, outliers in flux data were detected using the Tukey's interquartile range method (Wilks, 2011). In addition, strongly positive CO_2 fluxes during the day and strongly negative CO_2 fluxes at night were also removed. Only the data points that passed all these filtering criteria were kept in the final data for analysis. After the filtering, 73.9% of COS flux observations and 54.3% of CO_2 flux observations were retained.

2.5 Calculation of flux-derived variables

2.5.1 Stomatal conductance of water and total conductances of CO_2 and COS

Stomatal conductance of water (g_{s,H_2O}, mol m^{-2} s^{-1}) is calculated from water flux measurements,

$$g_{s,H_2O} = \frac{F_{H_2O}}{D} \tag{5}$$

where F_{H_2O} is the water flux (mmol m^{-2} s^{-1}), D is the leaf-to-air water vapor deficit expressed in mole fraction (mmol mol^{-1}). The mole-fraction vapor deficit D is calculated from

$$D = \frac{e_{sat}(T_{leaf})}{p} - \chi_{H_2O} \tag{6}$$

where e_{sat} (Pa) is the saturation water vapor pressure as a function of temperature (Goff and Gratch, 1946), T_{leaf} (°C) is the leaf temperature (see the Supplement for details), p (Pa) is the ambient pressure, and χ_{H_2O} (mmol mol^{-1}) is the water vapor mixing ratio in the chamber air.

The total conductances of COS ($g_{tot,COS}$, mol m^{-2} s^{-1}) and CO_2 (g_{tot,CO_2}, mol m^{-2} s^{-1}) are calculated from:

$$g_{tot,COS} = -\frac{F_{COS}}{\chi_{COS}} \tag{7}$$

$$g_{tot,CO_2} = -\frac{F_{CO_2}}{\chi_{CO_2}} \tag{8}$$

where F_{COS} (pmol m^{-2} s^{-1}) and F_{CO_2} (µmol m^{-2} s^{-1}) are leaf COS and CO_2 fluxes, χ_{COS} (pmol mol^{-1}) and χ_{CO_2} (µmol mol^{-1}) are mixing ratios of COS and CO_2 in the chamber air, respectively. Note that the intercellular concentrations of COS and CO_2 are canceled out from these equations by approximating their biochemical reaction rates with hypothetical (but mathematically convenient) 'biochemical conductances' (Stimler et al., 2010; Berry et al., 2013), which are then included in the total conductances.

2.5.2 Instantaneous and time-integrated leaf relative uptake ratios

Instantaneous leaf COS : CO_2 relative uptake (LRU) is defined as the ratio of COS and CO_2 fluxes normalized by their respective mixing ratios (Sandoval-Soto et al., 2005; Campbell et al., 2008; Whelan et al., 2017),

$$\mathrm{LRU} = \frac{F_{COS}}{F_{CO_2}} \cdot \frac{\chi_{CO_2}}{\chi_{COS}}, \text{ where } F_{COS} < 0 \text{ and } F_{CO_2} < 0 \tag{9}$$

LRU is a dimensionless quantity. We confine our LRU analysis to occasions where both COS and CO_2 fluxes are negative (i.e., showing net uptake). Hence, LRU is only calculated during the daytime and is always positive.

We also calculate the all-day mean LRU ($\mathrm{LRU_{all\text{-}day}}$) and the daytime mean LRU ($\mathrm{LRU_{daytime}}$) of each day using

$$\mathrm{LRU_{all\text{-}day}} = \frac{\left(\sum_{i=0}^{23} F_{\mathrm{COS}}^{i}\right) \cdot \left(\sum_{i=0}^{23} \chi_{\mathrm{CO_2}}^{i}\right)}{\left(\sum_{i=0}^{23} F_{\mathrm{CO_2}}^{i}\right) \cdot \left(\sum_{i=0}^{23} \chi_{\mathrm{COS}}^{i}\right)} \tag{10}$$

$$\mathrm{LRU_{daytime}} = \frac{\left(\sum_{i=6}^{19} F_{\mathrm{COS}}^{i}\right) \cdot \left(\sum_{i=6}^{19} \chi_{\mathrm{CO_2}}^{i}\right)}{\left(\sum_{i=6}^{19} F_{\mathrm{CO_2}}^{i}\right) \cdot \left(\sum_{i=6}^{19} \chi_{\mathrm{COS}}^{i}\right)} \tag{11}$$

where i is the truncated hour number (integer), in local daylight-saving time (UTC–7). The daytime period is determined with solar elevation angle > 0°, which translates roughly to between 06:00 and 20:00. In each period of calculation, missing data points are gap-filled with the mean in that period.

2.5.3 Contributions of stomatal component to the total resistance

To assess the relative importance of the stomatal limitation on COS and CO_2 uptake with respect to internal limitations (mesophyll conductance and biochemical reactions), we calculate the ratios of stomatal resistance to total resistance for COS (r^{*}_{COS}) and CO_2 ($r^{*}_{\mathrm{CO_2}}$),

$$r^{*}_{\mathrm{COS}} = \frac{r_{\mathrm{s,\,COS}}}{r_{\mathrm{tot,\,COS}}} = \frac{g_{\mathrm{tot,\,COS}}}{g_{\mathrm{s,\,COS}}} = \frac{g_{\mathrm{tot,\,COS}}}{g_{\mathrm{s,\,H_2O}}/2.01} \tag{12}$$

$$r^{*}_{\mathrm{CO_2}} = \frac{r_{\mathrm{s,\,CO_2}}}{r_{\mathrm{tot,\,CO_2}}} = \frac{g_{\mathrm{tot,\,CO_2}}}{g_{\mathrm{s,\,CO_2}}} = \frac{g_{\mathrm{tot,\,CO_2}}}{g_{\mathrm{s,\,H_2O}}/1.66} \tag{13}$$

where 2.01 is the water-to-COS ratio of diffusivity in air, and 1.66 is the water-to-CO_2 ratio of diffusivity in air (Seibt et al., 2010). The reason to switch from conductance to its reciprocal—resistance—is simply that different resistance components are additive.

2.6 Fitting light response curves for leaf COS and CO_2 fluxes and LRU

We used the LOWESS (locally weighted scatterplot smoothing) regression method to obtain smooth light response curves for COS flux, CO_2 flux, and LRU (see Fig. 5). The LOWESS regression method is a nonparametric method that does not require any a priori known relationship between the predictor (here, PAR) and the response variables (COS flux, CO_2 flux, and LRU). At each point in the range of the predictor, a low-degree polynomial is fitted to all the neighboring points to estimate the least squares response, weighted by the distances between the neighboring points and the current point (Cleveland et al., 1992). The calculation was performed with the Python statsmodels package (Seabold and Perktold, 2010).

3 Results

3.1 Leaf fluxes of COS, CO_2, and water

During the campaign period in June 2013 covering the peak growing season of *Typha latifolia*, meteorological conditions changed little except for a few cloudy days (8, 9, and 30 June 2013 in Fig. 2d), and the diurnal patterns of leaf COS, CO_2, and H_2O fluxes therefore also remained similar (Fig. 2a–c). The diurnal patterns of leaf fluxes and related variables are visualized with hourly binned medians and quartiles (Fig. 3).

In the daytime, leaf uptake of COS and CO_2 showed similar patterns (Fig. 3a, b), with uptake peaks in the morning and afternoon separated by a prolonged midday depression around local noon (13:00). The midday depression was up to 36% for COS (5.5 pmol m^{-2} s^{-1} at 14 h versus 8.5 pmol m^{-2} s^{-1} at 11 h) and 40% for CO_2 (3.7 µmol m^{-2} s^{-1} at 13 h versus 6.1 µmol m^{-2} s^{-1} at 17 h), respectively. The morning peaks coincided for the two fluxes at around 11:00, whereas the afternoon peak occurred a bit later for COS (18:00) than for CO_2 (17:00). The afternoon peak of CO_2 flux was slightly stronger than its morning peak (Fig. 3b, c), probably because the chamber received slightly more light in the afternoon than in the morning (Fig. 3e) due to a wider gap in the canopy to the west of the chamber than to other directions. Leaf transpiration showed a decline at 11:00 (Fig. 3c), but with an earlier afternoon peak (16:00) that coincided with the maximum vapor deficit (Fig. 3f). Contrary to COS and CO_2 fluxes, the diurnal pattern of water flux was strongly asymmetric due to the high vapor deficit in the afternoon (Fig. 3f).

In contrast to daytime fluxes, nighttime fluxes of COS and CO_2 showed diverging patterns. At night, CO_2 was emitted from leaf respiration (Fig. 3b), whereas COS uptake continued (Fig. 3a). Both fluxes had significantly smaller magnitudes than during the day, with CO_2 emissions of around 1 µmol m^{-2} s^{-1}, and COS uptake of around 2–3 pmol m^{-2} s^{-1}. Note that although COS emissions were occasionally observed at night (Fig. 2a), they were likely caused by random error due to high flow rates (~6 slm), and the hourly medians indeed showed a robust pattern of nighttime COS uptake (Fig. 3a). When averaged over the whole campaign, nighttime COS uptake was 23% of the total daily COS uptake by leaves. Nighttime transpiration was minimal (Fig. 3c) as the vapor deficit was close to zero at night (Fig. 3f).

COS flux was overall well correlated with CO_2 flux, with an r^2 of 0.49 (Fig. 4a), reaffirming the shared stomatal control on both fluxes. The correlation between COS and water fluxes was lower, r^2 = 0.32 (Fig. 4b), and showed a wide spread in the daytime due to the asymmetric diurnal pattern of water fluxes (Fig. 3c). At night, COS fluxes showed larger variability than water fluxes because vapor deficit that drives transpiration was small (Fig. 3f).

The midday depression was also evident in the light responses of fluxes. Both COS and CO_2 uptake rates increased with PAR until they became light saturated, and then decreased at high light and high vapor deficit (Fig. 5a, b). According to the smoothed light response curves, at a typical midday light level (1800 µmol m^{-2} s^{-1}), COS uptake drops by 37% from the peak value of 7.5 pmol m^{-2} s^{-1} (at PAR = 493 µmol m^{-2} s^{-1}) to 4.7 pmol m^{-2} s^{-1}, while CO_2 uptake drops by 31% from the peak value of 5.3 µmol m^{-2} s^{-1} (at PAR = 740 µmol m^{-2} s^{-1}) to 3.7 pmol m^{-2} s^{-1}. This indicates that stomatal conductance exerted a stronger control on COS uptake than CO_2 uptake.

3.2 Diurnal patterns of stomatal conductance and total conductance

Stomatal conductance ($g_{s,\,H_2O}$) derived from water measurements showed a distinct period of midday depression in its diurnal pattern (Fig. 6a). $g_{s,\,H_2O}$ was the highest in the early morning after daybreak, but started to drop quickly as the vapor deficit picked up, reaching its minimum at local noon (13:00). In the late afternoon, stomatal conductance slowly rebounded and remained relatively stable, but was still lower than the early morning level. Nighttime stomatal conductance was unable to be estimated from water measurements due to large uncertainty introduced by low vapor deficit and water flux.

The total conductance of COS ($g_{tot,\,COS}$) exhibited broadly similar diurnal pattern to that of $g_{s,\,H_2O}$, but lagged by 1 hour (Fig. 6a). This difference may be attributed to changes in internal conductance terms entailed in $g_{tot,\,COS}$, namely, mesophyll conductance and biochemical activities. A midday depression period was also visible in the diurnal trend of $g_{tot,\,COS}$. At night, $g_{tot,\,COS}$ remained at a stable, low level.

The ratios of stomatal resistance to total resistance of COS (r^*_{COS}) and of CO_2 ($r^*_{CO_2}$) indicated that stomatal limitation was the dominant component in the diffusional pathways of both gases during most of the daytime (Fig. 6b). For COS, stomatal limitation is always a much stronger component compared with that of CO_2. However, at around 15:00 the difference between stomatal limitation on COS uptake and that on CO_2 uptake was small (Fig. 6b).

3.3 Leaf relative uptake ratios

The instantaneous leaf relative uptake (LRU) showed an asymmetric U-shape diurnal pattern (Fig. 3d). LRU had highest values of 2–3 (medians binned by the hour) near dawn or dusk, with a gradual decrease throughout the morning and early afternoon, and then had minima around 0.9 at 15:00.

The diurnal pattern of LRU (Fig. 3d) was consistent with the LRU response to PAR (Fig. 5c). With increasing PAR, LRU decreased to around 1.0 at PAR above 500–600 μmol m^{-2} s^{-1} (Fig. 5c). Surprisingly, the lowest LRU values during the day did not occur at the time of the highest PAR (Fig. 3d), but rather at the time of the highest vapor deficit (Fig. 3f) and moderately strong PAR (1000–1400 μmol m^{-2} s^{-1}) due to the stronger stomatal limitation on fluxes as a response to the high vapor deficit. The timing of the lowest LRU (Fig. 3d), around 15:00, was when the difference between stomatal limitation on COS uptake and that on CO_2 uptake became the smallest (cf. Fig. 6b). However, this vapor deficit control on LRU was only secondary to the light control and was not evident in the light response of LRU (Fig. 5c).

The all-day mean LRU at this site showed large day-to-day variations (1.4–3.6) and also had large uncertainty due to the random error in nighttime CO_2 fluxes (Fig. 7a). In contrast, the daytime mean LRU, averaged over the daylight period of 14 hours, did not show strong variability (1.0–1.8) and had an average value of 1.2 across the campaign. The daytime mean LRU was consistently lower than the all-day mean LRU, since the latter included nighttime COS uptake and CO_2 emissions (Fig. 7a). Daytime mean LRU and daytime mean PAR was moderately well correlated ($r = -0.525$; Fig. 7b), similar to Maseyk et al. (2014). On overcast days, the daytime mean LRU values were higher than on clear days (Fig. 7a), as is expected from the light response of LRU. This indicates that the LRU–PAR relationship is preserved on the daily timescale.

4 Discussion

4.1 Competition between stomatal and internal limitations underlie the responses of leaf relative uptake to light and vapor deficit

Using the ratio of stomatal resistance to total resistance as a metric of the relative importance of stomatal limitation (Fig. 6b), we can recognize how the dynamics of stomatal vs. internal limitations regulates LRU. At the leaf scale, LRU manifests the ratio between the stomatal limitation on COS uptake (r^*_{COS}) and that on CO_2 uptake ($r^*_{\mathrm{CO_2}}$) (compare Eqs. 12 and 13 to Eq. 9):

$$\mathrm{LRU} \equiv \frac{g_{\mathrm{tot,\,COS}}}{g_{\mathrm{tot,\,CO_2}}} = \frac{0.83 \cdot r^*_{\mathrm{COS}}}{r^*_{\mathrm{CO_2}}} \tag{14}$$

where 0.83 is the COS-to-CO_2 ratio of diffusivity in air (Seibt et al., 2010). The equation shows that LRU becomes smaller when r^*_{COS} and $r^*_{\mathrm{CO_2}}$ get closer, providing a simple mechanistic interpretation of LRU variability.

We have reaffirmed in field conditions that LRU decreases with increasing PAR (Fig. 5c), consistent with laboratory studies and ecosystem field studies (Stimler et al., 2010, 2011; Maseyk et al., 2014; Commane et al., 2015). This light response of LRU arises from the difference between the marginal gain (i.e., partial derivative) of COS uptake and that of CO_2 uptake with respect to the same increase of PAR (Fig. 5a, b). Increasing PAR drives an increase in CO_2 assimilation rates, which in turn leads to an increase in stomatal conductance to facilitate optimal CO_2 uptake. This increase in stomatal conductance also enables higher COS uptake rates, but as COS hydrolysis is light independent (Protoschill-Krebs et al., 1996), there is a proportionally greater increase in CO_2 than COS uptake. That LRU light response is chiefly due to differential biochemical limitations on COS and CO_2 uptake is supported by indirect evidence in r^*_{COS} and $r^*_{\mathrm{CO_2}}$ (Fig. 6b). For instance, from 06:00 to 13:00 with increasing PAR, the higher relative increase of $r^*_{\mathrm{CO_2}}$ than that of r^*_{COS} (Fig. 6b) indicated that the extent to which non-stomatal resistance reduces—attributed mainly to the increases in biochemical reaction rates—is higher for CO_2 than for COS.

In addition to PAR, vapor deficit has been identified as a secondary environmental driver of LRU. Stomatal response to vapor deficit, such as the midday depression (Fig. 6a), is a well-known behavior that serves to optimize water use against carbon gain (e.g., Tenhunen et al., 1984; Collatz et al., 1991). However, the fact that vapor deficit has differential effects on COS and CO_2 uptake appears puzzling, since it does not affect differently COS and CO_2 biochemical reactions, and nor is it known to affect mesophyll conductance. A closer scrutiny of the stomatal limitations of COS and CO_2 (Fig. 6b) shows that the difference between r^*_{COS} and $r^*_{\mathrm{CO_2}}$ became smaller during the period of peak vapor deficit (14:00–17:00). Although vapor deficit has the same effect on $g_{\mathrm{s,\,COS}}$ and $g_{\mathrm{s,\,CO_2}}$, it can change the proportion of stomatal vs. internal components in the total resistance to the uptake, because COS uptake is always more stomatal-conductance-limited than CO_2 uptake (r^*_{COS} always higher than $r^*_{\mathrm{CO_2}}$ in Fig. 6b)—a consequence of the higher catalytic efficiency ($k_{\mathrm{cat}}/K_{\mathrm{m}}$) of β-CA in COS hydrolysis (Protoschill-Krebs et al., 1996; Ogée et al., 2016) than RuBisCO in CO_2 fixation (Tcherkez et al., 2006). Thus, vapor deficit controls LRU variability, but is less influential than PAR.

Since the mesophyll conductance is also a component in the internal conductance, it is worthy of note that the increase of mesophyll conductance with leaf temperature (Bernacchi, 2002) may have contributed to the dynamics of stomatal vs. internal

limitations over the course of the daytime, as is shown in Wehr et al. (2017), although we lack relevant data to separate biochemical limitation from mesophyll limitation.

4.2 Nighttime COS uptake is a significant portion of COS budget

During this campaign, nighttime uptake contributed to 23% of the total daily leaf COS uptake. This fraction is comparable to those reported from a wheat field (29 ± 5%, Maseyk et al., 2014), an alpine temperate forest (25–30%, Berkelhammer et al., 2014), a boreal pine forest (17%, Kooijmans et al., 2017), and a New England mixed forest (< 20% after subtracting soil uptake, Commane et al., 2015; Wehr et al., 2017). Collectively, these studies indicate that nighttime uptake is typically 17–30% of the total canopy COS budget, a fraction too large to be ignored in ecosystem or regional COS budget. Understanding nighttime COS uptake is necessary for the success of COS-based photosynthesis estimates on daily and longer timescales.

The *T. latifolia* leaves showed a mean value of 5.0 mmol m^{-2} s^{-1} for the total conductance of COS ($g_{tot,\,COS}$) at night (Fig. 6a). Assuming that the internal conductance of COS at night is the same as its daytime average, we obtain an estimate of nighttime $g_{s,\,COS}$, 6.4 mmol m^{-2} s^{-1} (see the Supplement for detailed calculations). This estimate of the nighttime $g_{s,\,COS}$ is at the lower end of values reported from other ecosystems: 1.6 mmol m^{-2} s^{-1} for a New England mixed forest (Wehr et al., 2017), 5–30 mmol m^{-2} s^{-1} for a Scots pine forest (Kooijmans et al., 2017), 11.5 mmol m^{-2} s^{-1} for a wheat field (Maseyk et al., 2014), and 13–20 and 22–66 mmol m^{-2} s^{-1} for pine and poplar trees, respectively, in an alpine temperate forest (Berkelhammer et al., 2014). The nighttime stomatal conductance shows a large variability among different species.

In land biosphere models, nighttime stomatal conductance is often a fixed value regardless of plant type and water status, e.g., $g_{s,\,H_2O}$ = 10 mmol m^{-2} s^{-1} in the Community Land Model v4.5 (Oleson et al., 2013). The fixed-value parameterization may introduce biases to the nighttime COS fluxes and long-term COS budget in regional simulations, which may in turn propagate into the COS-based photosynthesis estimates. To constrain nighttime COS uptake requires an understanding of the variability of nighttime stomatal conductance among plant species and ecosystem types. Water and COS flux measurements need to be used in conjunction to derive robust estimates of nighttime stomatal conductance. We expect COS measurements to be particularly useful for stomatal conductance estimates in tropical rainforests and other environments that experience high humidity conditions, provided that the variability of the internal conductance of COS is well understood.

4.3 Implications on COS-based GPP estimation

LRU is an important empirical parameter used to derive GPP from COS measurements on spatial scales ranging from the ecosystem to the continent (Asaf et al., 2013; Commane et al., 2015; Hilton et al., 2015). Choosing a representative LRU for COS-based GPP estimation is crucial and challenging.

In addition to its environmental controls, LRU also varies among plant species (Stimler et al., 2012). For the *T. latifolia*, the asymptotic LRU value at high light (PAR > 600 μmol m^{-2} s^{-1}) is around 1.0 (Fig. 5c). This value is much lower than the mean LRU of 1.61 ± 0.26 from laboratory measurements across a range of species (Stimler et al., 2012), which has been used as a representative LRU in ecosystem-scale (e.g., Asaf et al., 2013) and regional-scale GPP inversion studies (e.g., Hilton et al., 2015). The low asymptotic LRU of *T. latifolia* is, however, not surprising according to the mechanistic LRU model in Seibt

et al. (2010), which describes that LRU is positively related to the ratio of intercellular CO_2 to the ambient CO_2 (C_i/C_a). Since *T. latifolia* often has a high photosynthetic capacity (e.g., Tinoco Ojanguren and Goulden, 2013; Jespersen et al., 2017), as a result, its C_i/C_a ratio may be lower than other species, thus contributing to the low LRU. Relatively low LRU values have also been reported from other ecosystems, for example, 1.3 in a wheat field (Maseyk et al., 2014) and 1.2 in a mixed temperate forest at high PAR (Commane et al., 2015). This suggests that for the success of COS-based GPP estimation, LRU needs to be locally constrained on the dominant species in an ecosystem, rather than assumed to be a constant.

For regional scale applications, the time-integrated LRU can be more relevant than the instantaneous LRU. Large scale patterns of COS and CO_2 drawdown imprinted in an air parcel are spatiotemporally integrated features, because the transport of surface uptake signals to the planetary boundary layer takes time and may be affected by the entrainment with other parcels along the way. Our results of time-integrated LRU show that although daytime mean LRU and PAR are correlated, nighttime leaf respiration and COS uptake create large variability in the all-day mean LRU, which decouples it from PAR (Fig. 7b). This suggests that a bottom-up scaling is unlikely to offer reliable daily LRU values for regional scale applications. Instead, LRU that is diagnostically calculated from biosphere models such as the Simple Biosphere model (Berry et al., 2013; Hilton et al., 2015) would be more appropriate for COS–GPP inversion studies, provided that model parameterizations are validated against observations.

5 Conclusions

Our field study has shown that leaf COS and CO_2 fluxes share similar diurnal patterns driven by the common stomatal responses to light and vapor deficit, showing dual peaks of uptake separated by a prolonged midday depression period. We have validated the light dependence of LRU directly at the leaf level in field conditions. LRU converges to around 1.0 at light-saturated conditions for *Typha latifolia*, much lower than many other species due possibly to its high photosynthetic capacity. In addition to light, vapor deficit is identified as a secondary driver of LRU, acting to reduce LRU further in the afternoon (15:00–17:00) from its light-saturated value.

Stomatal conductance derived from water measurements has provided process-level insights into the diurnal variability of LRU. Since the biochemical sink of COS is light independent, COS uptake is less reaction-limited compared with CO_2 uptake. With increasing light, the assimilation capacity for CO_2 increases but is unchanged for COS, causing LRU to decrease regardless of the stomatal coupling between COS and CO_2. The reduction in stomatal conductance induced by high vapor deficit affects COS uptake more than CO_2 uptake, since COS uptake is more stomatal-conductance-limited, causing a further reduction in LRU. In a word, LRU variability is regulated by the relative influences of stomatal limitation vs. internal limitation on COS and CO_2 uptake.

The coupling between leaf COS and CO_2 fluxes and the predictability of LRU lend strong support to the use of COS as a quantitative tracer of canopy photosynthesis. More unknowns exist in the process-level controls of LRU, especially the variability of internal conductance. We expect that future studies may find the use of LRU as a diagnostic of stomatal processes to be interesting.

Data availability. Data presented here can be found in the University of California Curation Center (UC3) Merritt data repository at https://doi.org/10.15146/R37T00.

Author contributions. U.S. designed and supervised the research. All authors conducted the fieldwork. W.S. and U.S. performed data analysis. W.S., U.S., and K.M. wrote the paper with contributions from all co-authors.

Competing interests. The authors declare no conflict of interest.

Acknowledgements. The work was performed at the San Joaquin Freshwater Marsh (SJFM) Reserve of the University of California Natural Reserve System. We thank Mike Goulden at UC Irvine for help and discussions, and Bill Bretz and Peter Bowler for assistance at the SJFM UC Reserve. This work was supported by the European Research Council (ERC) Starting Grant no. 202835 and NSF CAREER Award no. 1455381 to U.S.

References

Asaf, D., Rotenberg, E., Tatarinov, F., Dicken, U., Montzka, S. A., and Yakir, D.: Ecosystem photosynthesis inferred from measurements of carbonyl sulphide flux, Nature Geoscience, 6, 186–190, https://doi.org/10.1038/ngeo1730, 2013.

Ball, J. T.: An analysis of stomatal conductance, Ph.D. thesis, Stanford University, 1988.

Berkelhammer, M., Asaf, D., Still, C., Montzka, S., Noone, D., Gupta, M., Provencal, R., Chen, H., and Yakir, D.: Constraining surface carbon fluxes using in situ measurements of carbonyl sulfide and carbon dioxide, Global Biogeochemical Cycles, 28, 161–179, https://doi.org/10.1002/2013GB004644, 2014.

Bernacchi, C. J.: Temperature response of mesophyll conductance. Implications for the determination of Rubisco enzyme kinetics and for limitations to photosynthesis in vivo, Plant Physiology, 130, 1992–1998, https://doi.org/10.1104/pp.008250, http://dx.doi.org/10.1104/pp.008250, 2002.

Berry, J., Wolf, A., Campbell, J. E., Baker, I., Blake, N., Blake, D., Denning, A. S., Kawa, S. R., Montzka, S. A., Seibt, U., Stimler, K., Yakir, D., and Zhu, Z.-X.: A coupled model of the global cycles of carbonyl sulfide and CO_2: A possible new window on the carbon cycle, Journal of Geophysical Research: Biogeosciences, 118, 842–852, https://doi.org/10.1002/jgrg.20068, 2013.

Billesbach, D. P., Berry, J. A., Seibt, U., Maseyk, K., Torn, M. S., Fischer, M. L., Abu-Naser, M., and Campbell, J. E.: Growing season eddy covariance measurements of carbonyl sulfide and CO_2 fluxes: COS and CO_2 relationships in Southern Great Plains winter wheat, Agricultural and Forest Meteorology, 184, 48–55, https://doi.org/10.1016/j.agrformet.2013.06.007, 2014.

Campbell, J. E., Carmichael, G. R., Chai, T., Mena-Carrasco, M., Tang, Y., Blake, D. R., Blake, N. J., Vay, S. A., Collatz, G. J., Baker, I., Berry, J. A., Montzka, S. A., Sweeney, C., Schnoor, J. L., and Stanier, C. O.: Photosynthetic Control of Atmospheric Carbonyl Sulfide During the Growing Season, Science, 322, 1085–1088, https://doi.org/10.1126/science.1164015, 2008.

Campbell, J. E., Whelan, M. E., Seibt, U., Smith, S. J., Berry, J. A., and Hilton, T. W.: Atmospheric carbonyl sulfide sources from anthropogenic activity: Implications for carbon cycle constraints, Geophysical Research Letters, 42, 3004–3010, https://doi.org/10.1002/2015GL063445, 2015GL063445, 2015.

Campbell, J. E., Berry, J. A., Seibt, U., Smith, S. J., Montzka, S. A., Launois, T., Belviso, S., Bopp, L., and Laine, M.: Large historical growth in global terrestrial gross primary production, Nature, 544, 84–87, https://doi.org/10.1038/nature22030, 2017.

Cleveland, W. S., Grosse, E., and Shyu, W. M.: Chapter 8 Local Regression Models, in: Statistical Models in S, edited by Chambers, J. M. and Hastie, T. J., Wadsworth & Brooks/Cole, Pacific Grove, California, USA, 1992.

Collatz, G. J., Ball, J. T., Grivet, C., and Berry, J. A.: Physiological and environmental regulation of stomatal conductance, photosynthesis and transpiration: a model that includes a laminar boundary layer, Agricultural and Forest Meteorology, 54, 107–136, https://doi.org/10.1016/0168-1923(91)90002-8, 1991.

Commane, R., Meredith, L. K., Baker, I. T., Berry, J. A., Munger, J. W., Montzka, S. A., Templer, P. H., Juice, S. M., Zahniser, M. S., and Wofsy, S. C.: Seasonal fluxes of carbonyl sulfide in a midlatitude forest, Proceedings of the National Academy of Sciences, 112, 14 162–14 167, https://doi.org/10.1073/pnas.1504131112, 2015.

Goff, J. A. and Gratch, S.: Low-pressure properties of water from −160 to 212°F, in: The 52nd Annual Meeting of the American Society of Heating and Ventilating Engineers, pp. 95–122, New York, USA, 1946.

Goldan, P. D., Fall, R., Kuster, W. C., and Fehsenfeld, F. C.: Uptake of COS by growing vegetation: A major tropospheric sink, Journal of Geophysical Research: Atmospheres, 93, 14 186–14 192, https://doi.org/10.1029/JD093iD11p14186, 1988.

Goulden, M. L., Litvak, M., and Miller, S. D.: Factors that control *Typha* marsh evapotranspiration, Aquatic Botany, 86, 97–106, https://doi.org/10.1016/j.aquabot.2006.09.005, 2007.

Hilton, T. W., Zumkehr, A., Kulkarni, S., Berry, J., Whelan, M. E., and Campbell, J. E.: Large variability in ecosystem models explains uncertainty in a critical parameter for quantifying GPP with carbonyl sulphide, Tellus B, 67, 26 329, https://doi.org/10.3402/tellusb.v67.26329, 2015.

Hilton, T. W., Whelan, M. E., Zumkehr, A., Kulkarni, S., Berry, J. A., Baker, I. T., Montzka, S. A., Sweeney, C., Miller, B. R., and Campbell, J. E.: Peak growing season gross uptake of carbon in North America is largest in the Midwest USA, Nature Climate Change, 7, 450–454, https://doi.org/10.1038/nclimate3272, 2017.

Jespersen, E., Brix, H., and Sorrell, B. K.: Acclimation to light and avoidance of photoinhibition in Typha latifolia is associated with high photosynthetic capacity and xanthophyll pigment content, Functional Plant Biology, 44, 774–784, https://doi.org/10.1071/fp16356, http://dx.doi.org/10.1071/FP16356, 2017.

Kooijmans, L. M. J., Uitslag, N. A. M., Zahniser, M. S., Nelson, D. D., Montzka, S. A., and Chen, H.: Continuous and high-precision atmospheric concentration measurements of COS, CO_2, CO and H_2O using a quantum cascade laser spectrometer (QCLS), Atmospheric Measurement Techniques, 9, 5293–5314, https://doi.org/10.5194/amt-9-5293-2016, 2016.

Kooijmans, L. M. J., Maseyk, K., Seibt, U., Sun, W., Vesala, T., Mammarella, I., Kolari, P., Aalto, J., Franchin, A., Vecchi, R., Valli, G., and Chen, H.: Canopy uptake dominates nighttime carbonyl sulfide fluxes in a boreal forest, Atmospheric Chemistry and Physics, 17, 11 453–11 465, https://doi.org/10.5194/acp-17-11453-2017, 2017.

Launois, T., Belviso, S., Bopp, L., Fichot, C., and Peylin, P.: A new model for the global biogeochemical cycle of carbonyl sulfide–Part 1: Assessment of direct marine emissions with an oceanic general circulation and biogeochemistry model, Atmospheric Chemistry and Physics, 15, 2295–2312, https://doi.org/10.5194/acp-15-2295-2015, 2015.

Leuning, R.: A critical appraisal of a combined stomatal–photosynthesis model for C3 plants, Plant, Cell & Environment, 18, 339–355, https://doi.org/10.1111/j.1365-3040.1995.tb00370.x, 1995.

Maseyk, K., Berry, J. A., Billesbach, D., Campbell, J. E., Torn, M. S., Zahniser, M., and Seibt, U.: Sources and sinks of carbonyl sulfide in an agricultural field in the Southern Great Plains, Proceedings of the National Academy of Sciences, 111, 9064–9069, https://doi.org/10.1073/pnas.1319132111, 2014.

Montzka, S., Calvert, P., Hall, B., Elkins, J., Conway, T., Tans, P., and Sweeney, C.: On the global distribution, seasonality, and budget of atmospheric carbonyl sulfide (COS) and some similarities to CO_2, Journal of Geophysical Research, 112, D09 302, https://doi.org/10.1029/2006JD007665, 2007.

Nelson, D.: TDLWintel User's Manual, Aerodyne Research, Inc., Billerica, MA, USA, 2012.

Notni, J., Schenk, S., Protoschill-Krebs, G., Kesselmeier, J., and Anders, E.: The missing link in COS metabolism: a model study on the reactivation of carbonic anhydrase from its hydrosulfide analogue, ChemBioChem, 8, 530–536, https://doi.org/10.1002/cbic.200600436, 2007.

Ogawa, T., Noguchi, K., Saito, M., Nagahata, Y., Kato, H., Ohtaki, A., Nakayama, H., Dohmae, N., Matsushita, Y., Odaka, M., Yohda, M., Nyunoya, H., and Katayama, Y.: Carbonyl sulfide hydrolase from *Thiobacillus thioparus* strain THI115 is one of the β-carbonic anhydrase family enzymes, Journal of the American Chemical Society, 135, 3818–3825, https://doi.org/10.1021/ja307735e, 2013.

Ogée, J., Sauze, J., Kesselmeier, J., Genty, B., Van Diest, H., Launois, T., and Wingate, L.: A new mechanistic framework to predict OCS fluxes from soils, Biogeosciences, 13, 2221–2240, https://doi.org/10.5194/bg-13-2221-2016, 2016.

Oleson, K. W., Lawrence, D. M., Bonan, G. B., Drewniak, B., Huang, M., Koven, C. D., Levis, S., Li, F., Riley, W. J., Subin, Z. M., Swenson, S., Thornton, P. E., Bozbiyik, A., Fisher, R., Heald, C. L., Kluzek, E., Lamarque, J.-F., Lawrence, P. J., Leung, L. R., Lipscomb, W., Muszala, S. P., Ricciuto, D. M., Sacks, W. J., Sun, Y., Tang, J., , and Yang, Z.-L.: Technical description of version 4.5 of the Community Land Model (CLM), NCAR Technical Report NCAR/TN-503+STR, National Center for Atmospheric Research (NCAR), Boulder, CO, USA, https://doi.org/10.5065/D6RR1W7M, 2013.

Protoschill-Krebs, G., Wilhelm, C., and Kesselmeier, J.: Consumption of carbonyl sulphide (COS) by higher plant carbonic anhydrase (CA), Atmospheric Environment, 30, 3151–3156, https://doi.org/10.1016/1352-2310(96)00026-X, 1996.

Sandoval-Soto, L., Stanimirov, M., Hobe, M. v., Schmitt, V., Valdes, J., Wild, A., and Kesselmeier, J.: Global uptake of carbonyl sulfide (COS) by terrestrial vegetation: Estimates corrected by deposition velocities normalized to the uptake of carbon dioxide (CO_2), Biogeosciences, 2, 125–132, https://doi.org/10.5194/bg-2-125-2005, 2005.

Schenk, S., Kesselmeier, J., and Anders, E.: How does the exchange of one oxygen atom with sulfur affect the catalytic cycle of carbonic anhydrase?, Chemistry – A European Journal, 10, 3091–3105, https://doi.org/10.1002/chem.200305754, 2004.

Seabold, S. and Perktold, J.: Statsmodels: Econometric and Statistical Modeling with Python, in: The 9th Python in Science Conference, 2010.

Seibt, U., Kesselmeier, J., Sandoval-Soto, L., Kuhn, U., and Berry, J.: A kinetic analysis of leaf uptake of COS and its relation to transpiration, photosynthesis and carbon isotope fractionation, Biogeosciences, 7, 333–341, https://doi.org/10.5194/bg-7-333-2010, 2010.

Stimler, K., Montzka, S. A., Berry, J. A., Rudich, Y., and Yakir, D.: Relationships between carbonyl sulfide (COS) and CO_2 during leaf gas exchange, New Phytologist, 186, 869–878, https://doi.org/10.1111/j.1469-8137.2010.03218.x, 2010.

Stimler, K., Berry, J. A., Montzka, S. A., and Yakir, D.: Association between carbonyl sulfide uptake and ^{18}O during gas exchange in C_3 and C_4 leaves, Plant Physiology, 157, 509–517, https://doi.org/10.1104/pp.111.176578, 2011.

Stimler, K., Berry, J. A., and Yakir, D.: Effects of carbonyl sulfide and carbonic anhydrase on stomatal conductance, Plant physiology, 158, 524–530, https://doi.org/10.1104/pp.111.185926, 2012.

Tcherkez, G. G. B., Farquhar, G. D., and Andrews, T. J.: Despite slow catalysis and confused substrate specificity, all ribulose bisphosphate carboxylases may be nearly perfectly optimized, Proceedings of the National Academy of Sciences, 103, 7246–7251, https://doi.org/10.1073/pnas.0600605103, http://dx.doi.org/10.1073/pnas.0600605103, 2006.

Tenhunen, J. D., Lange, O. L., Gebel, J., Beyschlag, W., and Weber, J. A.: Changes in photosynthetic capacity, carboxylation efficiency, and CO_2 compensation point associated with midday stomatal closure and midday depression of net CO_2 exchange of leaves of *Quercus suber*, Planta, 162, 193–203, https://doi.org/10.1007/BF00397440, 1984.

Tinoco Ojanguren, C. and Goulden, M. L.: Photosynthetic acclimation within individual Typha latifolia leaf segments, Aquatic Botany, 111, 54–61, https://doi.org/10.1016/j.aquabot.2013.08.007, http://dx.doi.org/10.1016/j.aquabot.2013.08.007, 2013.

Wehr, R., Commane, R., Munger, J. W., McManus, J. B., Nelson, D. D., Zahniser, M. S., Saleska, S. R., and Wofsy, S. C.: Dynamics of canopy stomatal conductance, transpiration, and evaporation in a temperate deciduous forest, validated by carbonyl sulfide uptake, Biogeosciences, 14, 389–401, https://doi.org/10.5194/bg-14-389-2017, 2017.

Whelan, M., Lennartz, S., Gimeno, T., Wehr, R., Wohlfahrt, G., Wang, Y., Kooijmans, L., Hilton, T., Belviso, S., Peylin, P., Commane, R., Sun, W., Chen, H., Kuai, L., Mammarella, I., Maseyk, K., Berkelhammer, M., Li, K.-F., Yakir, D., Zumkehr, A., Katayama, Y., Ogée, J., Spielmann, F., Kitz, F., Rastogi, B., Kesselmeier, J., Marshall, J., Erkkilä, K.-M., Wingate, L., Meredith, L., He, W., Bunk, R., Launois, T., Vesala, T., Schmidt, J., Fichot, C., Seibt, U., Saleska, S., Saltzman, E., Montzka, S., Berry, J., , and Campbell, J. E.:

Reviews and Syntheses: Carbonyl Sulfide as a Multi-scale Tracer for Carbon and Water Cycles, Biogeosciences Discussions, 2017, 1–97, https://doi.org/10.5194/bg-2017-427, 2017.

Wilks, D. S.: Statistical Methods in the Atmospheric Sciences, Academic Press, 3rd edn., 2011.

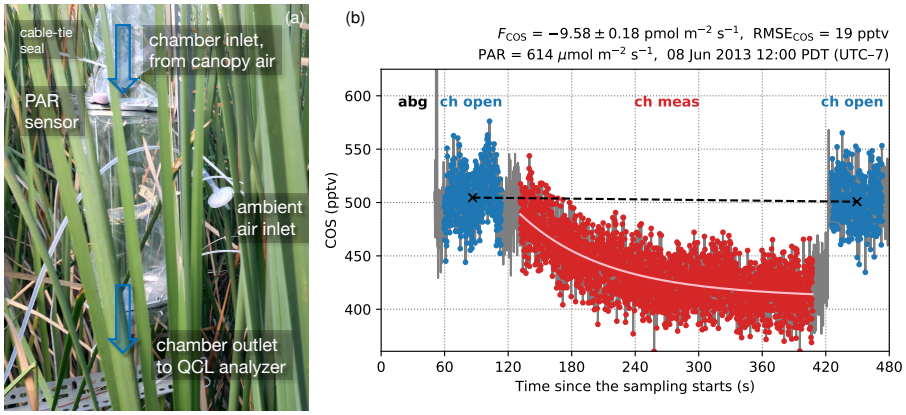

Figure 1. (a) A schematic diagram of the leaf chamber. (b) A typical sampling period on the leaf chamber illustrated with COS concentration measurements. The first minute is for auto-background spectral correction (abg) using N_2 gas. The sampling system then switches to the chamber line with the ventilation fan turned on (ch open) for one minute. Then the ventilation fan is turned off for five minutes to measure flux signals in the chamber (ch meas), and after that is turned on again for one minute (ch open). The fitted curve for concentration changes is shown in light pink. The black dashed line represents the zero-flux baseline correction to account for the drift in the measured ambient concentrations.

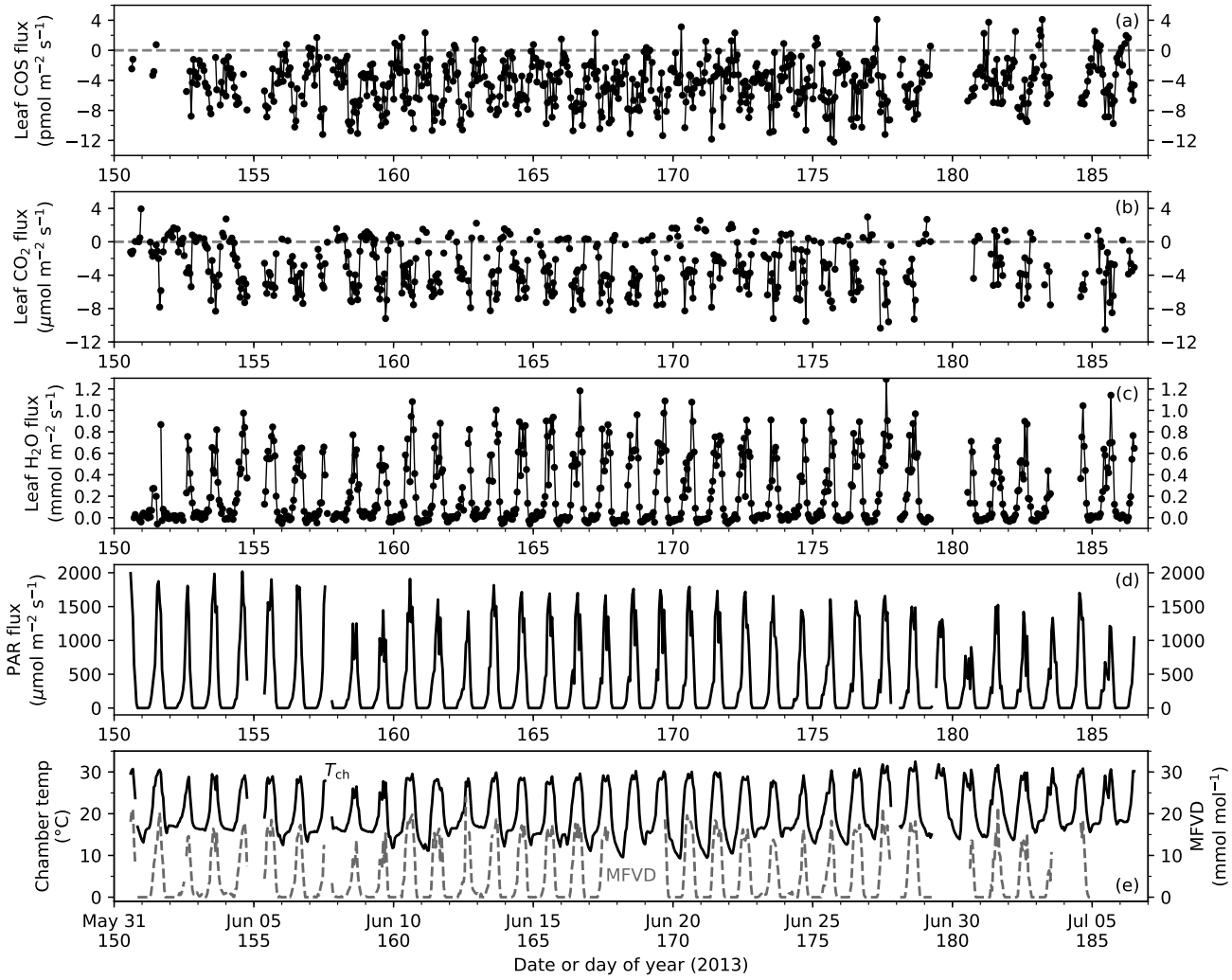

Figure 2. Time series of leaf COS (a), CO_2 (b) and water (c) fluxes, photosynthetically active radiation (PAR) at the leaf chamber (d), chamber air temperature (e, black solid line; T_{ch}) and leaf-to-air vapor deficit in mole fraction (e, gray dashed line; MFVD). Ticks on x-axes indicate the starts of the days (0000 h).

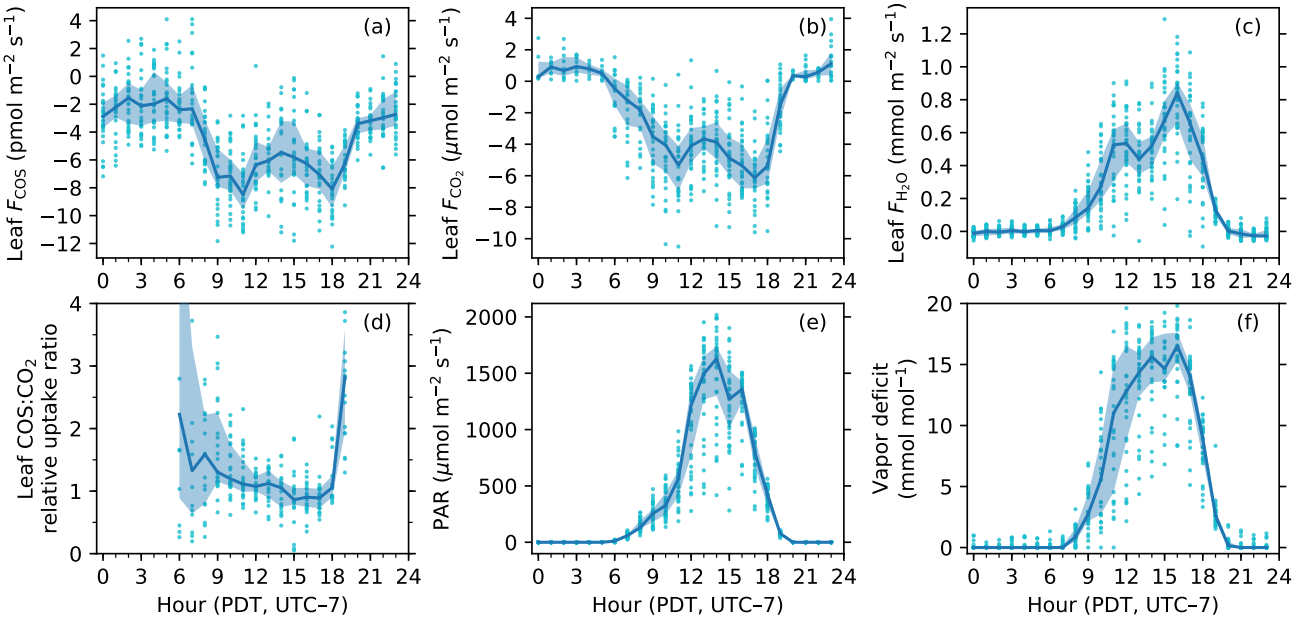

Figure 3. Diurnal patterns of leaf COS (a), CO_2 (b) and water (c) fluxes, leaf relative uptake ratio (d), PAR at the leaf chamber (e), and leaf-to-air vapor deficit in mole fraction (f). The solid curves show medians binned by the hour of the day (Pacific Daylight Time, UTC–7), and the upper and lower bounds of shaded areas are 25th and 75th percentiles, respectively.

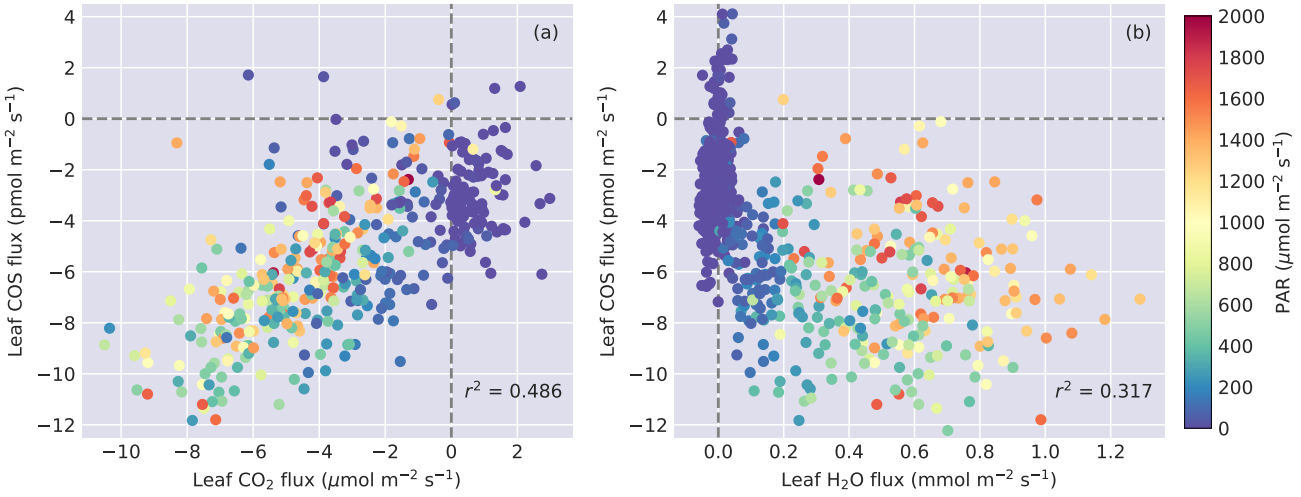

Figure 4. (a) Leaf COS vs. CO_2 fluxes, and (b) leaf COS vs. H_2O fluxes. Data points are colored by the PAR level.

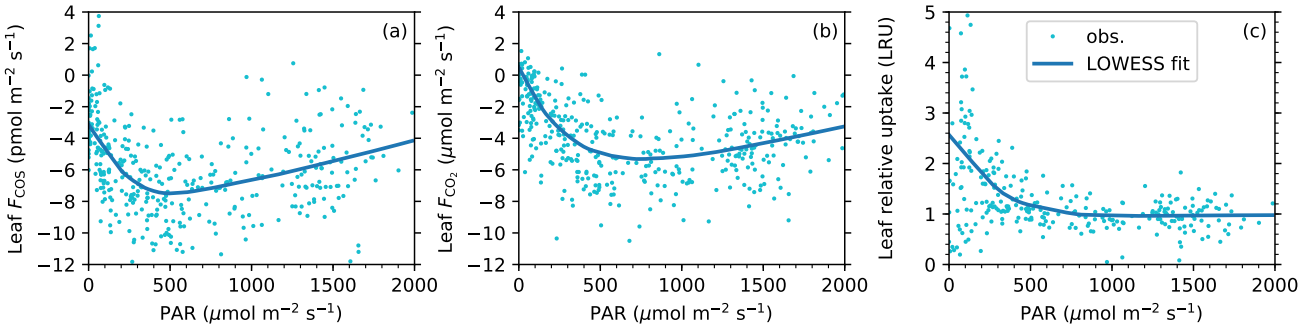

Figure 5. Light responses of leaf COS flux (a), CO_2 flux (b), and leaf relative uptake ratio (c). Data are shown as dots, and the smoothed curves are fitted with the nonparametric LOWESS method.

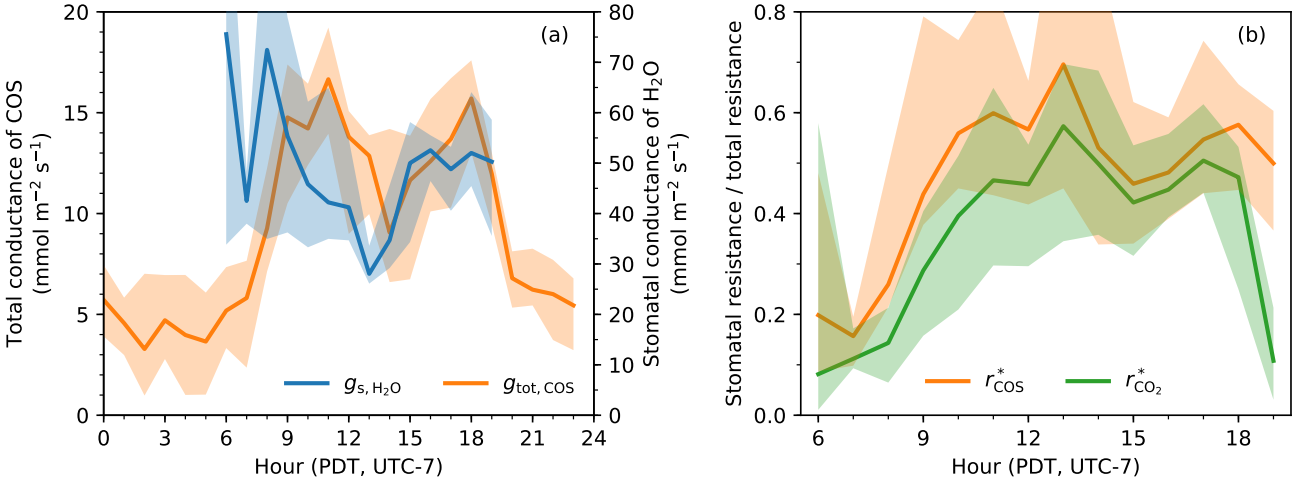

Figure 6. (a) Diurnal patterns of the stomatal conductance of water (blue, right y-axis) and the total conductance of COS (orange, left y-axis). Note that the two variables were on different scales for visual comparison. (b) Daytime patterns of the fraction of stomatal resistance in the total resistance for COS (orange) and for CO_2 (green). Similar to Fig. 3, in both panels solid curves indicate medians and shaded areas are between 25th and 75th percentiles, binned by the hour of the day.

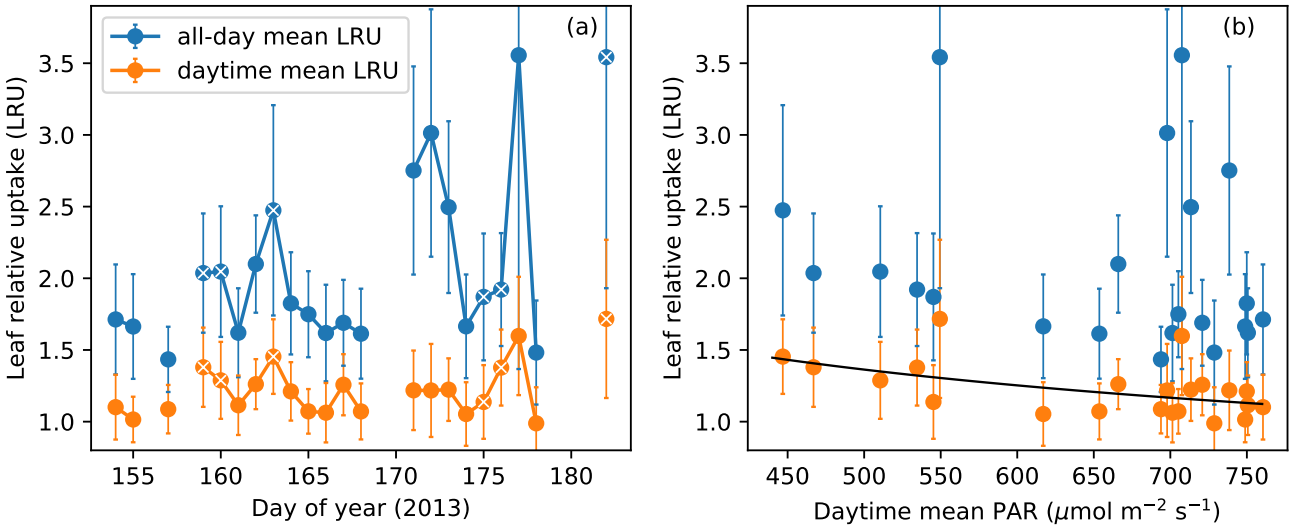

Figure 7. (a) All-day mean (blue) and daytime mean (orange) leaf relative uptake (LRU) ratios during the campaign. Data points from overcast days (daytime mean PAR < 550 μmol m^{-2} s^{-1}) are labeled with additional white cross signs. (b) All-day mean and daytime mean LRU values vs. daytime mean PAR. Daytime mean LRU vs. PAR follows a response curve (black): LRU = 24.0689 $PAR^{-0.4620}$. Error bars in both panels show ranges of ±1 standard error.

Table 1. List of variable symbols

Symbol	Description
χ_{COS}	COS mixing ratio (pptv or pmol mol^{-1})
χ_{CO_2}	CO_2 mixing ratio (ppmv or µmol mol^{-1})
χ_{H_2O}	H_2O mixing ratio (mmol mol^{-1})
F_{COS}	COS flux (pmol m^{-2} s^{-1})
F_{CO_2}	CO_2 flux (µmol m^{-2} s^{-1})
F_{H_2O}	H_2O flux (mmol m^{-2} s^{-1})
$g_{s,\,COS}$	Stomatal conductance of COS (mol m^{-2} s^{-1})
$g_{s,\,CO_2}$	Stomatal conductance of CO_2 (mol m^{-2} s^{-1})
$g_{s,\,H_2O}$	Stomatal conductance of water (mol m^{-2} s^{-1})
$r_{s,\,COS}$	Stomatal resistance of COS (mol^{-1} m^2 s)
$r_{s,\,CO_2}$	Stomatal resistance of CO_2 (mol^{-1} m^2 s)
$r_{s,\,H_2O}$	Stomatal resistance of water (mol^{-1} m^2 s)
$g_{tot,\,COS}$	Total conductance of COS (mol m^{-2} s^{-1})
$g_{tot,\,CO_2}$	Total conductance of CO_2 (mol m^{-2} s^{-1})
$r_{tot,\,COS}$	Total resistance of COS (mol^{-1} m^2 s)
$r_{tot,\,CO_2}$	Total resistance of CO_2 (mol^{-1} m^2 s)
$r^*_{CO_2}$	Ratio of stomatal resistance to total resistance of CO_2
r^*_{COS}	Ratio of stomatal resistance to total resistance of COS
T_{ch}	Chamber air temperature (°C)
T_{leaf}	Leaf temperature (°C)
e_{sat}	Saturation vapor pressure (Pa)
MFVD or D	Leaf-to-air vapor deficit in mole fraction (mmol mol^{-1})
LRU	Instantaneous leaf relative uptake
$LRU_{all\text{-}day}$	All-day mean leaf relative uptake
$LRU_{daytime}$	Daytime mean leaf relative uptake